Title: **Ghosts of a structured past: Impacts of ancestral patterns of isolation-by-distance on divergence-time estimation**

Running Title: Impacts of ancestral IBD on divergence-times

Zachary B. Hancock[*1,2], Heath Blackmon[1,2]

[1]Department of Biology at Texas A&M University

[2]Ecology & Evolutionary Biology Interdisciplinary Program at Texas A&M University

*Corresponding author: zhancock@bio.tamu.edu

Author contributions: HB conceptualized the study; ZBH performed the analyses; ZBH and HB wrote the manuscript.

Acknowledgements: Thanks to Ben Haller and Wesley Brashear for coding help.

Data accessibility statement: SLiM recipes, R and python code, and .XML files have been uploaded to https://github.com/hancockzb/ancestralIBD.

19 Title: **Ghosts of a structured past: Impacts of ancestral patterns of isolation-by-distance on**
20 **divergence-time estimation**

21

22 **Abstract**

23 Isolation by distance is a widespread pattern in nature that describes the reduction of genetic
24 correlation between subpopulations with increased geographic distance. In the population
25 ancestral to modern sister species, this pattern may hypothetically inflate population divergence
26 time estimation due to the potential for allele frequency differences in subpopulations at the ends
27 of the ancestral population. In this study, we analyze the relationship between the time to the
28 most recent common ancestor and the population divergence time when the ancestral population
29 model is a linear stepping-stone. Using coalescent simulations, we compare the coalescent time
30 to the population divergence time for various ratios of the divergence time over the product of
31 the population size and the deme number. Next, we simulate whole genomes to obtain SNPs, and
32 use the Bayesian coalescent program SNAPP to estimate divergence times. We find that as the
33 rate of migration between neighboring demes decreases, the coalescent time becomes
34 significantly greater than the population divergence time when sampled from end demes.
35 Divergence-time overestimation in SNAPP becomes severe when the divergence-to-population
36 size ratio < 10 and migration is low. We conclude that studies estimating divergence times be
37 cognizant of the potential ancestral population structure in an explicitly spatial context or risk
38 dramatically overestimating the timing of population splits.

39

40 Keywords: Phylogenetics, divergence-time, isolation-by-distance

Introduction

A major goal in phylogenetic and phylogeographic studies is the estimation of species divergence times. The topic has a long and contentious history largely centered around questions of how to appropriately apply fossil calibrations (e.g., Heath et al. 2014; Brown and Smith 2018), rate heterogeneity (Pond and Muse 2005), rate of morphological evolution (Lynch 1990), and selecting an adequate clock model (Douzery et al. 2004; Lepage et al. 2007).

Beyond methodological concerns are those that emerge from the nature of the data itself. Most phylogenetic models assume that fixed differences between species are the result of genetic drift, and under the neutral theory of molecular evolution (Kimura 1968; King and Jukes 1969) the rate of evolution (or substitution rate) is equal to the per generation neutral mutation rate, μ (Kimura 1983). For well-calibrated molecular clocks (e.g., Knowlton and Weigt 1998; Weir and Schluter 2008; Herman et al. 2018), we can estimate the time of divergence (usually in years) as $\pi_{12} / 2\mu$, where π_{12} is the pairwise sequence divergence between species 1 and 2. However, in general we are not interested in estimating the divergence time of specific genetic variants, but rather the time of population divergence (T_D). For example, we might be interested in estimating the timing of a vicariant event that we suspect corresponds to a past geological upheaval.

There is a known discrepancy between the coalescent time of neutral genetic variants (T_{MRCA}) and T_D (Nei and Li 1979). The degree of this discrepancy is determined by the ratio of T_D / N_e, where N_e is the effective population size (Edwards and Beerli 2000; Rosenberg and Feldman 2002). First, lineages must be within the same population, which occurs T_D generations in the past; second, these lineages must then coalesce, which on average requires $2N_e$

63 generations. Therefore, for a completely panmictic population: $T_{MRCA} = T_D + 2N_e$. The expected
64 amount of pairwise sequence divergence is

65 $$E(\pi_{12}) = 2\mu[T_D + 2N_e] \quad (1)$$

66 (Wakeley 2000). When the ratio of T_D / N_e is large, the bias in coalescent time in the ancestral
67 population is minimal compared to T_D (Edwards and Beerli 2000). However, as T_D / N_e becomes
68 small, $2N_e$ plays a major role in the overall sequence divergence between species. Nordberg and
69 Feldman (2002) evaluated the relationship between T_{MRCA} and T_D in a simple two population
70 split model using coalescent simulations. They found that T_{MRCA} converged on T_D when the ratio
71 of $T_D / N_e \approx 5$. Importantly, the N_e in these models is that of the ancestral population; therefore,
72 the extent of overestimation is the result of demographic conditions present in the ancestor.
73 Demographic conditions that inflate N_e, such as ancestral population structure or a bottleneck
74 following the split, is expected to have a major impact on divergence-time estimation (Gaggiotti
75 and Excoffier 2000; Edwards and Beerli 2000; Wakeley 2000).

76 Wakeley (2000) demonstrated that in descendant species who share an ancestor whose
77 population dynamics are characterized by an island model (Wright 1931) with free migration
78 between demes, overestimation of divergence-times are on the order of $2N_eD[1 + (1/2M)]$ where
79 $M = 2N_emD/(D - 1)$ and m is the migration rate. The expected amount of pairwise sequence
80 divergence is therefore

81 $$E(\pi_{12}) = 2\mu\left[T_D + 2N_eD\left(1 + \frac{1}{2M}\right)\right] \quad (2)$$

82 where D is the number of demes.

83 Population subdivision initially leads to shallow coalescent times where individuals
84 within a shared deme rapidly find ancestors (the “scattering phase”). However, since ancestral
85 lineages must be in the same deme to coalesce, the rate in the “collecting phase” is characterized

by the migration rate that shuffles ancestors around the range, reducing the probability that lineages coalesce (Wakeley 1998; 1999).

In the context of real populations, the island model of migration rarely applies (Meirmans 2012). Instead, population structure is the product of the spatial distribution and dispersal potential of the organism in question. Often this structure is in the form of isolation-by-distance (IBD). IBD is a widespread pattern in natural systems, characterized by a reduction in the probability of identity by descent (Wright 1943) or genetic correlation (Malécot 1968) with geographic distance. Patterns of IBD are most pronounced in stepping-stone models (Kimura 1953; Kimura and Weiss 1964) in which migration is restricted to neighboring demes. In this way, demes in close proximity share a greater proportion of migrants than they do with more distant demes. Distributions of coalescent times in stepping-stone models have been studied both in the context of one dimensional and two-dimensional models that are circular or toroidal (Maruyama 1970a; 1970b; Slatkin 1991), and in continuous models with joined ends (Maruyama 1971) or with discrete edges (Wilkins and Wakeley 2002). Slatkin (1991), using a circular stepping-stone model, showed that the probability for two genes sampled i steps apart have an average coalescent time:

$$T_{MRCA} = 2N_eD + \frac{(D-i)i}{2m} \quad (3)$$

Therefore, the amount of expected pairwise sequence divergence is:

$$E(\pi_{12}) = 2\mu\left[T_D + 2N_eD + \frac{(D-i)i}{2m}\right] \quad (4)$$

The circular stepping-stone model should overestimate T_D more dramatically as the number of demes becomes large and the distance between them increases. However, like the island model of free migration, circular ranges are likely rare in nature. Instead, natural populations are characterized by discrete range edges where end demes may only receive

migrants from one direction (e.g., Peterson and Denno 1998; Broquet et al. 2006; Aguillon et al. 2017). Hey (1991) showed analytically in the case of a linear stepping-stone model that the distribution of coalescent times of two alleles from demes at the extremes of the range should coalesce much deeper than any two alleles chosen randomly from the population.

Ultimately, the degree to which T_{MRCA} impacts phylogenetic inference and divergence-time estimation is dependent on its impact on π_{12}. Given that lower migration rates lead to greater T_{MRCA} (Hey 1991), we expect that differentiation (π_{12}) between end demes compared to central will become more pronounced at smaller *m*. If the difference between the T_{MRCA} of central demes and end demes is dramatic enough, we expect that divergence dating of species that arose from ancestral end demes may significantly overestimate T_D. ##examples

In this study, we estimate mean T_{MRCA} for two genes sampled in descendant species (either from the ends or the center of the ancestral range) in which the ancestral population is characterized by a stepping-stone model with discrete ends using a simulation approach. In particular, we are interested in what value of T_D / *ND* we expect T_{MRCA} to converge on T_D. Next, we examine the distribution of π_{12} across the genome under different simulated migration conditions to compare with expectations under a panmictic model. Finally, we test the performance of the phylogenetic inference program SNAPP (Bryant et al. 2012) on simulated single nucleotide polymorphism (SNP) data to evaluate how these trends may bias our inference of species divergence times.

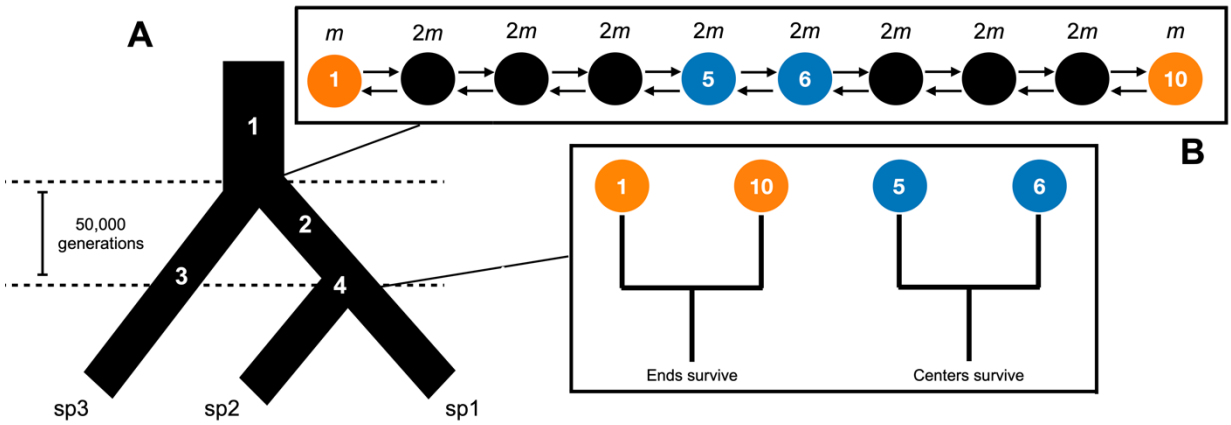

Figure 1. Population model for simulations. **A)** Three-taxon species tree: 1) coalescent simulations in *msprime* with $N = 2000$; 2) ancestral stepping-stone conditions begin (see **B**); 3) $N = 1000$, panmictic; 4) population split, leaving end or center demes surviving as sp1 and sp2. **B)** Ancestral population dynamics. Orange circles are "end demes" and blue circles are sampled "center" demes.

Methods

Coalescent simulations

Using *fastsimcoal2* (Excoffier et al. 2013), we simulated sister species with a shared ancestor whose population dynamics are characterized by a stepping-stone model. Specifically, each simulation consisted of 10 demes (D) with no shared migration between them until time T_D. At T_D, migration resumes between demes in a linear stepping-stone fashion. In *fastsimcoal2*, the migration rate is the probability of an individual from deme i migrating to deme j, where i and j are neighboring demes. Center demes receive migrants from neighboring demes at rate $2m$, whereas demes at the end of the range receive migrants at rate m. This is due to the fact that end demes have only a single neighbor, whereas all center demes have two neighbors (Fig. 1A).

Throughout, we will use "end demes" to represent species descending from the ends of the ancestral range; "center demes" are those that descend from the center. We sampled $k = 2$ individuals to coalesce—in one run, we sample the end demes, and in the following we sample central neighboring demes. This was performed for migration rates of 0.1, 0.01, and 0.001, and a range of T_D / *ND* values. In addition, we simulated an island model of migration for comparison with the stepping-stone model. In the island model, the ancestral population consisted of 10 demes with free migration between each at rate *m*. This resulted in a total of 84 distinct simulation scenarios, and each were replicated 1,000 times.

To statistically compare between the three models (end deme sampled in stepping-stone, center deme in stepping-stone, and the island model), we subset ratios of T_D / *ND* to values of 10, 5, 2, 1, 0.5, and 0.1. Resulting T_{MRCA} distributions for each population model were compared using a pairwise Wilcoxon test in the R platform (R Core Team 2019), as the resulting distributions were non-normal.

Genome simulations

To evaluate how ancestral IBD impacts pairwise sequence divergence (π_{12}), genome-wide coalescent times (T_{MRCA}), and divergence-time estimation, we performed hybrid simulations that combined the coalescent simulator *msprime* (Kelleher et al. 2016) and the forward-time simulator SLiM v3.3 (Haller and Messer 2019). Since forward-time simulators begin with individuals that are completely unrelated, often a neutral burn-in period is required to allow coalescence or mutation-drift equilibrium to occur (Haller et al. 2019). This can be computationally costly and time consuming; however, using tree-sequence recording methods in SLiM (Haller et al. 2019) we can bypass the need to equilibrate during the forward-time

simulation. To generate a panmictic ancestral population with a coalescent history, we simulated 2000 individuals (N_e = 4000) using *msprime* with genome sizes of 10 Mb and a recombination rate of 10^{-8} (~0.1 recombination events per individual per generation). The resulting coalescent trees were then imported into SLiM as the basis for the starting population.

In SLiM, the initial population was split into two populations of N = 1000: 1) an outgroup that remained panmictic ("sp3" in Fig. 1A) and 2) the ancestral population, which was subdivided into 10 demes (N = 100 per deme) in a linear stepping-stone model. These dynamics persisted for 50,000 generations after which the ancestral population was split into either "end" demes or "center" demes (see Fig. 1A). Population sizes of each deme following the split was increased to 1000 to maintain N throughout the simulation. Five different T_D values were simulated which correspond to T_D / ND ratios of 50, 25, 10, 5, and 1. These values of T_D / ND were chosen based on the results from the coalescent simulations (see Results); for values >10, T_{MRCA} is expected to converge on T_D, whereas values <10 are expected to overestimate T_D regardless of migration rates.

The resulting tree-sequences from the SLiM simulation were imported into Python 3 using *pyslim*, and we overlaid neutral mutations ($\mu = 10^{-7}$) onto the trees using *msprime*. Pairwise divergence (π_{12}) was then estimated across the genome in windows of 100 kb for both end demes and center demes. These values were also converted into generations using $\pi_{12} / 2\mu$, which gives a rough estimate of divergence time per window.

By rearranging equation 1, we can naively calculate N_e for the ancestral population from genome-wide π_{12} as:

$$N_e = \frac{\pi_{12} - 2T_D\mu}{4\mu} \quad (5)$$

From this, we plot estimated ancestral N_e within 100 kb windows across the genome to compare with the known census population size (N_c = 1000), and to evaluate the relationship between N_e and N_c in the presence of IBD.

Next, we plotted the distribution of coalescent times (T_{MRCA}) across the genome to visualize differences between T_{MRCA} of end and center demes. Median T_{MRCA} for each ratio and migration rate was compared via a Kruskal-Wallis test and a pairwise Wilcoxon rank test in R due to the data violating normality.

Each simulation produced >200,000 SNPs. For divergence-time analysis, we randomly sampled 3000 SNPs—a number found by Strange et al. (2018) to optimally perform in SNAPP (Bryant et al. 2012). Each run consisted of 10 individuals from species sp1 and sp2, and 1 individual from the outgroup population, sp3 (Fig. 1). Unlike other fully coalescent models, SNAPP does not sample from gene trees directly to estimate the species tree, but instead integrates over all possible gene trees using biallelic SNPs. The method has been found previously to perform well on both simulated and empirical data (Bryant et al. 2012; Strange et al. 2018). We designated a gamma-distributed prior on θ ($=4N_e\mu$) with a mean equal to the expected π_{12} (equation 1). Forward (u) and backward (v) mutation rates were estimated within BEAUti (Bouckaert et al. 2014) from the empirical SNP matrix using the tab *Calc_mutation_rates*, and these values were sampled during the MCMC. The rate parameter $\boldsymbol{\lambda}$, which is the birth-rate on the Yule tree prior, was gamma-distributed with $\alpha = 2$ and $\beta = 200$, where the mean is α / β (Leaché and Bouckaert 2018).

SNAPP is designed to handle incomplete lineage sorting (ILS), but to minimize its effects—since we are not interested in the program's ability to estimate topology but rather branch-lengths—we applied a fixed species tree. Branch-lengths in SNAPP do not scale to time,

but instead are measured in number of substitutions. Given a fixed mutation rate, we convert the number of substitutions separating sp1 and sp2 to the number of generations as $g = s / \mu$, where s is branch-lengths in units of substitutions (Bouckaert and Bryant 2015). The MCMC chain length was 10–50 million sampling every 1000 with a burn-in of 10%, ensuring that ESS values of interest were all >200. Runs were performed on the high-performance computing cluster CIPRES (www.phylo.org; Miller et al. 2010).

MCMC log files were then downloaded and analyzed in R. The performance of SNAPP was evaluated by comparing traces of end and center demes across migration rates and T_D / *ND* values. Results were evaluated using a two-way ANOVA followed by Tukey's HSD post hoc test in R. Trees from the MCMC were summarized in TreeAnnotator v.2.6.0 (Bouckaert et al. 2014) and visualized in R using the package *ggtree* (Yu et al. 2017). Branch colors and widths were scaled by estimated median θ per branch.

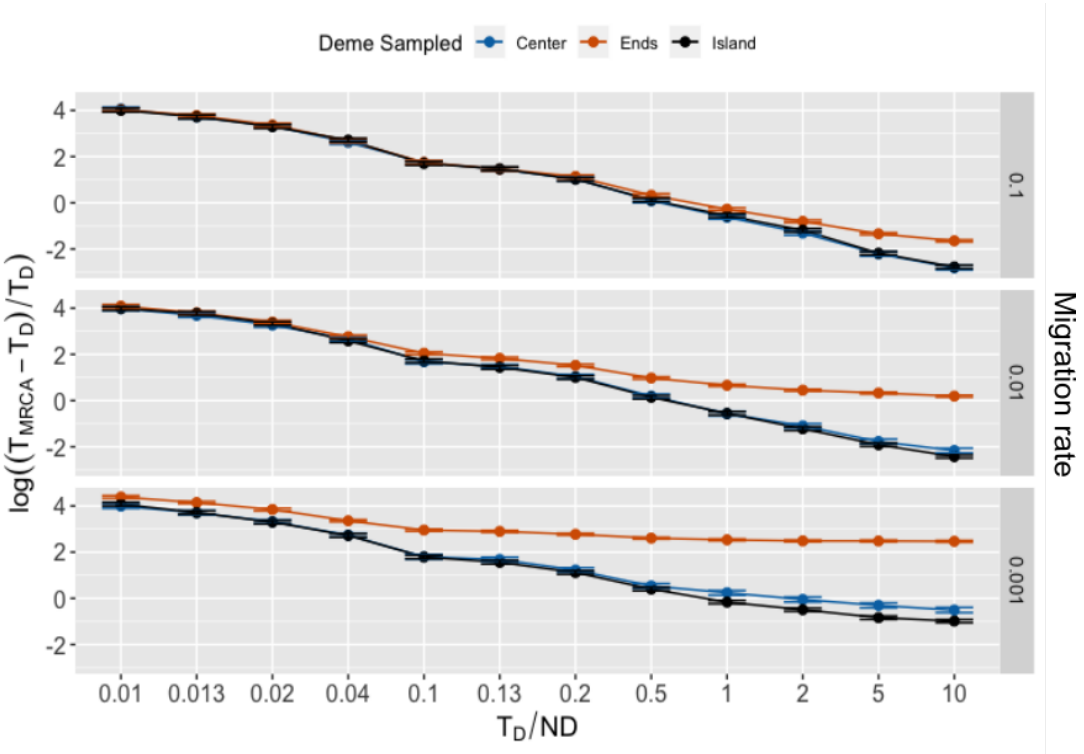

Figure 2. Plots of $\log((T_{MRCA} - T_D) / T_D)$ against T_D / ND for each migration rate (0.1, 0.01, 0.001). Each point is the mean of 1000 simulations. Y-axis has been log-transformed to aid in visualizing differences between model/deme sampled.

Results

Coalescent simulation results

The coalescent simulations produced trends superficially similar to those found by Rosenberg and Feldman (2002). At the lowest T_D / ND, the proportion of deep coalescence was dramatically greater than at higher values with the curve producing a similar logarithmic relationship (Fig. 2). However, T_D and T_{MRCA} did not necessarily converge when $T_D / ND = 5$. Instead, the rate of convergence was dependent on both the deme sampled and the migration rate.

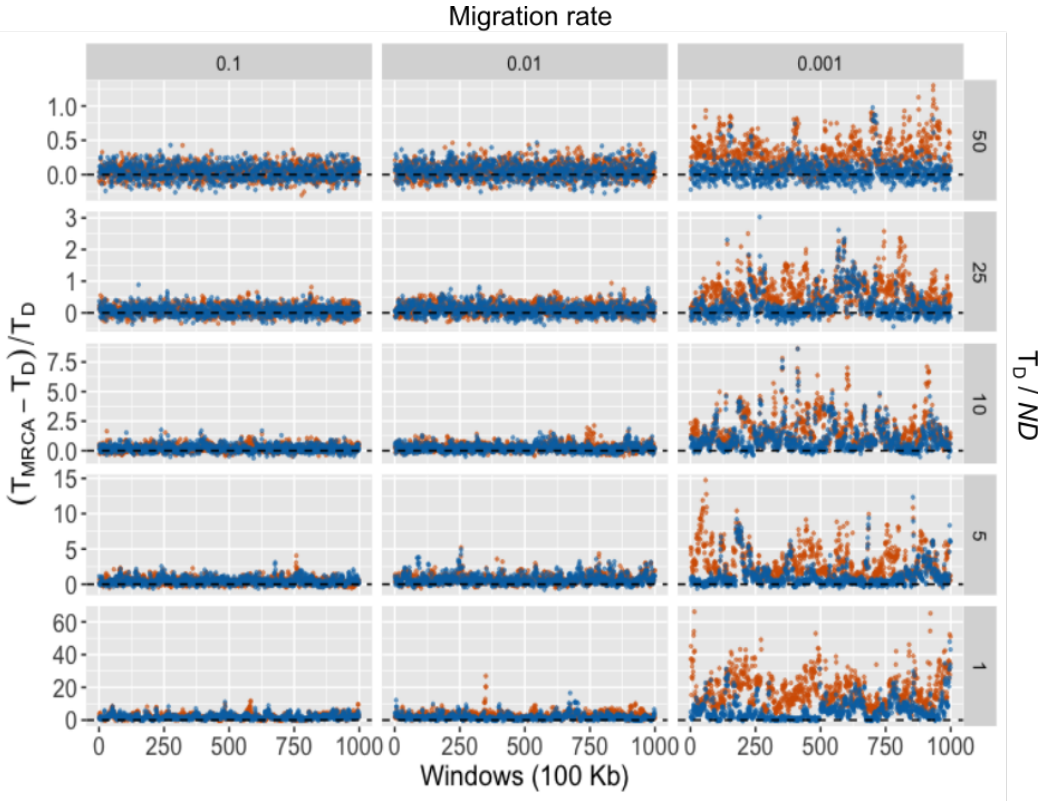

Figure 3. Genome-wide divergence times based on π_{12}. Divergence times are estimated as $\pi_{12} / 2\mu$ and evaluated in 100 Kb windows. The y-axis is the scaled proportion of overestimation, where T_{MRCA} is the estimated age and T_D is the true age. The dashed line represents the value at which these two converge (i.e., 0). Center (blue), ends (orange). Note the y-axis differs between the panels.

When migration was high ($m = 0.1$) and T_D / ND was less than 0.5, there was no significant difference between center or end demes in the stepping-stone model or the island model. However, for values of $T_D / ND > 0.5$, the T_{MRCA} of end demes became significantly different from both island ($p < 0.02$) and center demes ($p < 0.01$; see Table S1). When migration was reduced below 0.1, this pattern became more extreme. End demes were significantly different in all pairwise comparisons of models ($p < 0.000001$), and center demes differed from the island model at T_D / ND ratios of 0.5, 2, and 10 ($p < 0.03$) when $m = 0.01$. At the lowest migration rate simulated ($m = 0.001$), all pairwise model comparisons were significantly different when $T_D / ND > 0.5$ ($p < 0.001$; see Table S1).

Genome simulation results

Results from the genome simulation approach corroborated those found with *fastsimcoal2*. Regardless of T_D / ND, when $m = 0.1$ the difference between center and end demes was less severe and only marginally significant ($p = 0.001$) relative to when $m < 0.1$ (Table S2). Across the simulated genomes, T_{MRCA} became dramatically deeper between end than center demes as migration fell below 0.01. For the genome-wide divergence estimates, the degree of overestimation depended on the ratio of T_D / ND. While all scenarios where $m = 0.001$ overestimated the true T_D, when $T_D / ND < 10$ end demes were 5–60 times more diverged than

expected (Fig. 3). This is a direct result of the deeper coalescent times between end demes when $m < 0.1$, as these longer branches provide more time for mutations to occur and accumulate (Fig. 4).

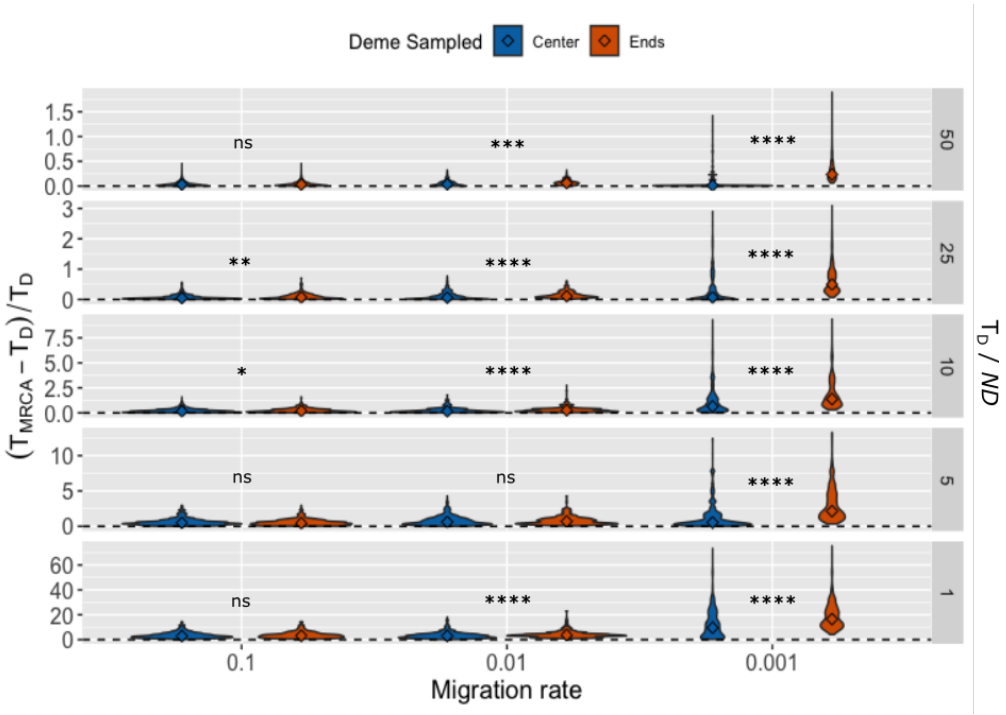

Figure 4. Violin plot of coalescent times (T_{MRCA}) across the genome, where times have been converted into proportions of the population divergence time (T_D). Diamonds are medians; ns = "not significant", $p < 0.05$ (*), $p < 0.001$ (**), $p < 0.0001$ (***), $p < 0.00001$ (****). See Table S2 for specific p-values. Note that the y-axis differs between panels.

Genome-wide coalescent times (T_{MRCA}) are shown in Fig. 4. When $m = 0.1$, only T_D / ND = 25 and 10 were significantly different between end and center demes ($p < 0.005$). Regardless of T_D / ND, the variance in T_{MRCA} steadily increased with decreasing m. Indeed, the increase in mean T_{MRCA} when $m = 0.001$ appears largely driven by an increase in the variance at this lower rate. Due to this, we find that ancestral N_e dramatically exceeds N_c when $m = 0.001$ (Fig. 6).

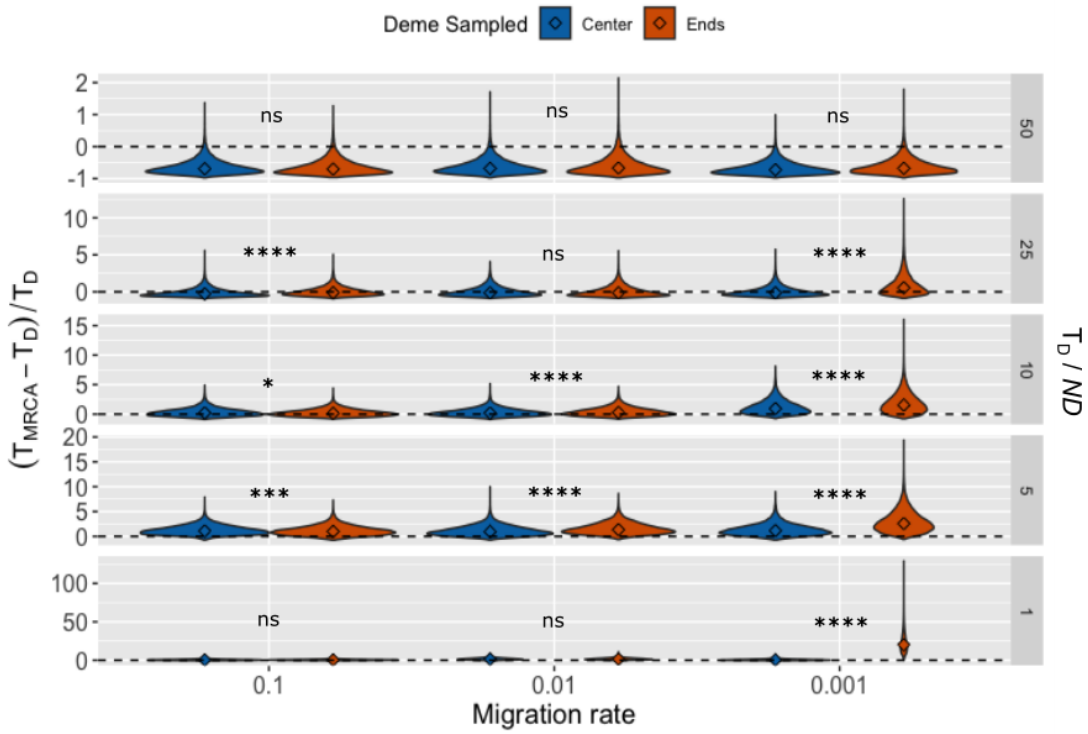

Figure 5. Violin plots of the estimated T_{MRCA} by SNAPP. Diamonds are medians; ns = "not significant", $p < 0.05$ (*), $p < 0.001$ (**), $p < 0.0001$ (***), $p < 0.00001$ (****). Dashed lines represent when the estimated age converges on the true age (i.e., at 0). Note that the y-axis is different between the panels.

Despite the potential for divergence-time overestimation to be extreme, SNAPP was relatively resilient when T_D / ND > 10 and when m > 0.001. When T_D / ND = 50, SNAPP was overly conservative and underestimated the number of substitutions expected to occur (Fig. 5). When T_D / ND = 25, the mean estimate of both center and end demes when m > 0.001 either underestimated the true age or was within 5%. However, for end demes where m = 0.001 the estimated divergence time exceeded the true age by ~80% (Table S3). A similar trend occurred when T_D / ND = 10 and 5. Here, both center and ends overestimated the true age, but the end demes did so more dramatically (138% the true age versus 81% for 10; 184% versus 67% for 5). The most dramatic overestimation occurred between end demes when T_D / ND = 1 at ~700% the true age. Importantly, this was not merely the result of a low T_D / ND ratio, as the other

290 migration regimes performed well. In fact, most were closer to the true T_D than the expected π_{12}
291 accounting for $2N$ (Table S3).

292 Estimated θ for each branch is shown in Fig. 7 for $T_D / ND = 10$, and in Figs. S1–S4 for
293 the remaining ratios. For all T_D / ND values except 1, the median ancestral θ was higher for end
294 demes than center when $m = 0.001$, and the estimated θ for the descendant species (sp1 and sp2
295 in Fig. 1) was considerably lower than for the ancestor or the outgroup, sp3 (Fig. 7; Figs. S1–S3).
296 These patterns are consistent with a population bottleneck, despite N being maintained
297 throughout the simulation.
298
299 **Discussion**
300
301 Macroevolutionary patterns are ultimately governed by microevolutionary processes (Li et al.
302 2018), an observation Lynch (2007), extending Dobzhansky's (1973) maxim, summed up as
303 "nothing in evolution makes sense except in light of population genetics". In this light, we have
304 demonstrated that the population genetic environment of the ancestor shapes the genetic
305 landscape of descendant species. This has been known to impact tree topology when ILS is
306 common (Kubatko and Degnan 2007) and overestimate divergence times in the presence of
307 population structure caused by an island model of migration (Edwards and Beerli 2000; Wakeley
308 2000). Extensive prior work has shown that the stepping-stone model of migration reduces
309 genetic correlation between demes (Kimura and Weiss 1964; Maruyama 1970a) and that demes
310 farther apart should coalesce deeper in time than those geographically closer (Slatkin 1991; Hey
311 1991). However, to our knowledge, the impact of ancestral IBD has not been evaluated in the
312 context of divergence-time estimation previously.

313 Rosenberg & Feldman (2002) found previously that when $T_D / N = 5$, T_{MRCA} and T_D
314 largely converged in a simple population split model. However, when in the presence of
315 ancestral IBD we found that convergence was dependent on the migration rate (i.e., the strength
316 of ancestral IBD) and whether surviving demes neighbored each other or were at the range ends
317 in the ancestral population.
318 When $T_D / ND > 10$, the ancestral dynamics contribute little to the divergence-time
319 estimate differences between center and end demes. However, as this ratio decreases the
320 contribution of $2N_e$ to overall sequence divergence becomes non-trivial. The probability that
321 genetic variants share an ancestor just prior to the population split is higher between demes that
322 are geographically closer than those more distant. This is mediated by the migration rate, which,
323 when high enough, can largely erase the differences between center and end demes. When
324 migration is high (10%, or $m = 0.1$), individuals move well between demes and the coalescent
325 times largely converge (though deeper in time depending on the ratio of T_D / ND). However, as
326 m falls below 1% ($m = 0.01$), or less than one migrant per generation being shared between
327 demes, dispersal cannot keep up with genetic differentiation. Despite all migration regimes
328 producing similar patterns of IBD (Fig. S5), F_{ST} becomes dramatically higher as migration drops
329 below 1%. This differentiation in the ancestor contributes to the overall sequence divergence
330 (π_{12}) between species, which drives an overestimation of the time of the population split (T_D)
331 when end demes are the surviving lineages.
332 As expected, ancestral IBD skews π_{12} and T_{MRCA} away from expected values in a
333 panmictic population, and this caused an inflation in N_e relative to N_c. For $T_D / ND = 50$ and $m =$
334 0.1, the mean π_{12} for end demes was 0.010459 and 0.010419 for center demes. Using equation 5,
335 $N_e = 1147.5$ for end demes and 1047.5 for central. However, when $m = 0.001$, π_{12} for end demes

was 0.012948, an N_e = 7370. Center demes, on the other hand, only increased to N_e = 1255. As with the coalescent times, at lower migration rates the variance in N_e becomes exceedingly large, driving up the mean. Importantly, mean genome-wide N_e always exceeds N_c in the presence of ancestral IBD at a level dictated by the migration rate.

This feature of ancestral IBD has important consequences for conservation genetics. Many studies use N_e as a rough biological measure of population size (Turner et al. 2002; Rieman and Allendorf, 2011; Hare et al. 2011), and therefore a metric of the health of a population. However, a common phenomenon in range contractions is fragmentation and isolation (Ceballos et al. 2017), which may result in IBD. If many of the demes once contributing to the connectivity of the population have become extinct, and N_e is estimated based on the surviving demes, it will overestimate the actual number of individuals within the population (i.e., the census size, N_c). Thus, we might incorrectly conclude that a population has a larger population size than it actually does, which may lead to mismanagement.

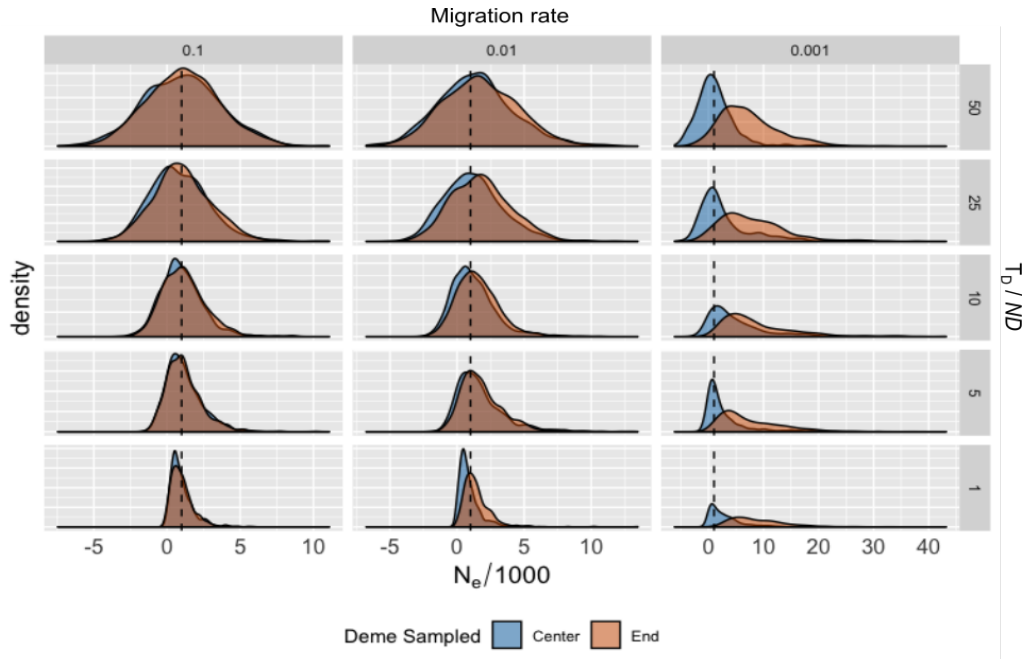

Figure 6. Density plot of scaled N_e (/1000) based on mean π_{12} across genomic windows of 100kb. Dashed line is when N_e / N_c = 1.

Since N_e is inflated in the ancestral lineage, the descendant species appear to pass through a bottleneck despite N remaining constant (Fig. 7). Estimated θ in SNAPP captured this dynamic with more extreme differences in θ (i.e., more dramatic bottlenecks) being inferred between end demes and when $m = 0.001$. Population bottlenecks have been found to cause divergence-time overestimation due to random differential survival of ancestral alleles into the descendant species (Gaggiotti and Excoffier 2000). In the presence of IBD, this differential allelic persistence between demes is mimicking a bottleneck—when demes are far apart this pattern is more extreme as they already maintain different allelic patterns ancestrally. However, because this pattern is recognizable (Fig. 7; Figs. S1–S3) it can be used to signal when ancestral IBD may be impacting our divergence-time estimation. Unfortunately, without prior range-size knowledge it may be impossible to differentiate between ancestral IBD and a bottleneck since these produce virtually identical genetic patterns. However, it may not be necessary to do so for simple divergence estimates.

The broader impact of ancestral IBD on divergence-time estimation when in the context of large phylogenies is beyond the scope of this work, but it is conceivable that the longer than expected branches between sister species might bias rate estimation (Aris-Brosou and Excoffier 1996; Magallón 2010). In the case of ancestral IBD, the inflated N_e is mimicking a pattern of substitution rate increase. Under neutrality, the rate of substitution is equal to the per generation mutation rate, μ (Kimura 1983); however, in the presence of population structure, substitutions may occur in the ancestral lineages between demes separated by large geographic distances. If

372 the true age of the sister taxa is known but ancestral structure is not accounted for, the
373 substitution rate will be upwardly biased.

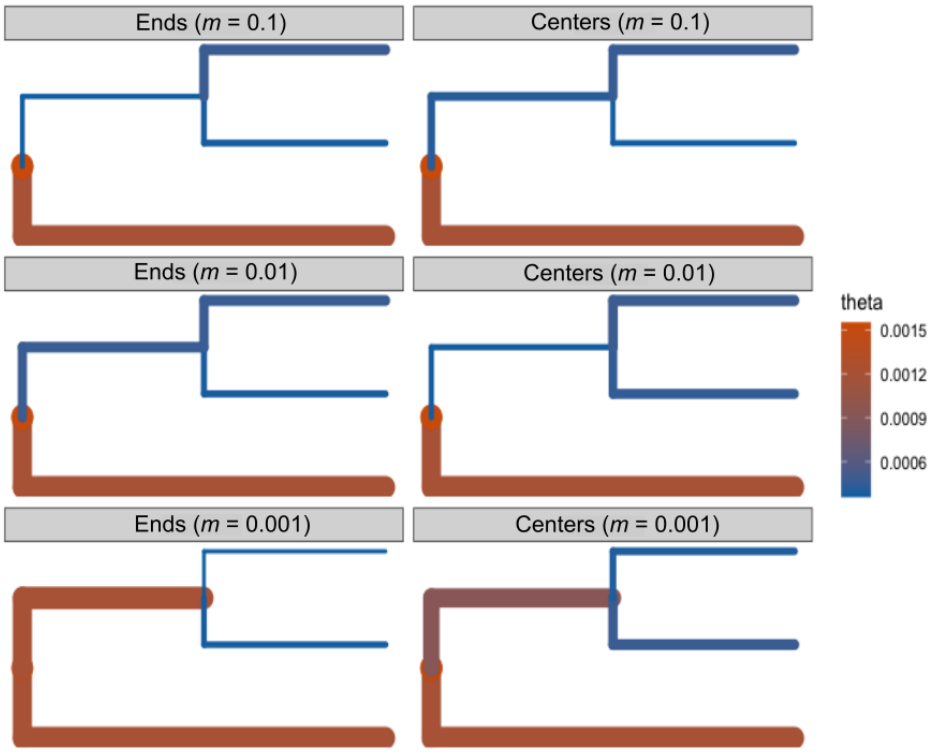

374

375 **Figure 7.** Estimates of θ in SNAPP for T_D / ND = 10. Branch widths are proportional to the estimated θ.

376

377 Ancestral structured populations leave their imprint on descendent species in the form of
378 greater coalescent times, and therefore larger than expected pairwise divergences between
379 species. Further, these patterns cause inflated N_e relative to census sizes. Since ancestral IBD
380 mimics the signature of a population bottleneck, coalescent methods that co-estimate θ along
381 with the topology and π_{12}, such as SNAPP and *BEAST (Bouckaert et al., 2014), may be the
382 best suited to reveal this potential source of bias. However, fully coalescent models such as these
383 are infamously computationally costly and not presently used for whole-genome sequence data

or for phylogenies with large numbers of tips. Indeed, SNAPP becomes prohibitively slow when the number of tips is ~30 (Leaché and Bouckaert, 2018).

In the context of larger phylogenies or organisms in which little is known about their ancestral range, it may be impossible to know if extant species descend from range centers or ends, or the level of IBD present in the ancestor. The genetic consequences of ancestral structure therefore behave much like "ghost" populations (Slatkin 2005); despite being extinct, their influence haunts our ability to adequately assess the phylogenetic history of their descendants.

References

Aguillon, S.M., Fitzpatrick, J.W., Bowman, R., Schoech, S.J., Clark, A.G., Coop, G., and N. Chen. 2017. Deconstructing isolation-by-distance: The genomic consequences of limited dispersal. PLoS Genet. 13(8): e1006911.

Aris-Brosou, S., and L. Excoffier. 1996. The impact of population expansion and mutation rate heterogeneity on DNA sequence polymorphism. Mol. Biol. Evo. 13(3): 494–504.

Bouckaert, R., and Bryant, D. 2015. A rough guide to SNAPP. https://www.beast2.org/snapp/

Bouckaert, R., Heled, J., Kühnert, D., Vaughan, T., Wu, C-H., Xie, D., Suchard, M.A., Rambaut, A., and Drummond, A.J. (2014). BEAST 2: A Software Platform for Bayesian Evolutionary Analysis. PLoS Comp. Bio. 10(4): e1003537.

Broquet, T., Ray, N., Petit, E., Fryxell, J.M., and F. Burel. 2006. Genetic isolation by distance and landscape connectivity in the American marten (*Martes americana*). Land. Eco. 21: 877–889.

Brown, J.W., and S.A. Smith. 2018. The past sure is tense: On interpreting phylogenetic divergence time estimates. Syst. Biol. 67(2): 340–353.

Bryant, D., Bouckaert, R., Felsenstein, J., Rosenberg, N.A. and A. RoyChoudhury. 2012. Inferring species trees directly from biallelic genetic markers: bypassing gene trees in a full coalescent analysis. Mol. Bio. Evo. 29(8): 1917–1932.

Ceballos, G., Ehrlich, P.R., and R. Dirzo. 2017. Biological annihilation via the ongoing sixth mass extinction signaled by vertebrate population losses and declines. PNAS. 114(30): E6089-E6096.

Dobzhansky, T. 1973. Nothing in biology makes sense except in the light of evolution. American Biology Teacher. 35: 125–129

Douzery, E.J.P., Snell, E.A., Bapteste, E., Delsuc, F., and H. Philippe. 2004. The timing of eukaryotic evolution: Does a relaxed molecular clock reconcile proteins and fossils? PNAS. 101(43): 15386–15391.

Edwards, S.V., and P. Beerli. 2000. Gene divergence, population divergence, and the variance in coalescent time in phylogeographic studies. Evolution. 54(6): 1839–1854.

Excoffier, L., Dupanloup, I., Huerta-Sánchez, E., Sousa, V.C., and M. Foll. 2013. Robust demographic inference from genomic and SNP data. PLoS Genet. 9(10): e1003905.

Gaggiotti, O.E., and L. Excoffier. 2000. A simple method for removing the effect of a bottleneck and unequal population sizes on pairwise genetic distances. Proc. B. 267(1438): 81–87.

Haller, B.C., and P.W. Messer. 2019. SLiM 3: Forward genetic simulations beyond the Wright-Fisher Model. Mol. Bio. Evo. 36(3): 632–637.

Haller, B.C., Galloway, J., Kelleher, J., Messer, P.W., and P.L. Ralph. 2019. Tree-sequence recording in SLiM opens new horizons for forward-time simulation of whole genomes. Mol. Eco. Res. 19(2): 552–566.

Hare, M.P., Nunney, L., Schwartz, M.K., Ruzzante, D.E., Burford, M., Waples, R.S., Ruegg, K., and F. Palstra. Understanding and Estimating Effective Population Size for Practical Application in Marine Species Management. 25(3): 438–449.

Heath, T.A., Hueslenbeck, J.P., and T. Stadler. 2014. The fossilized birth-death process for coherent calibration of divergence-time estimates. PNAS. E2957-E2966.

Herman, A., Brandvain, Y., Weagley, J., Jeffery, W.R., Keene, A.C., Kono, T.J.Y., Bilandžija, H., Borowsky, R., Espinasa, L., O'Quin, K., Ornelas-García, C.P., Yoshizawa, M., Carlson, B., Maldonado, E., Gross, J.B., Cartwright, R.A., Rohner, N., Warren, W.C., and S.E. McGaugh. 2018. The role of gene flow in rapid and repeated evolution of cave-related traits in Mexican tetra, *Astyanax mexicanus*. Mol. Eco. 27(22): 4397–4416.

Hey, J. 1991. A multi-dimensional coalescent process applied to multi-allelic selection models and migration models. Theo. Pop. Bio. 39: 30–48.

Kelleher, J., Etheridge, A.M., and G. McVean. 2016. Efficient Coalescent Simulation and Genealogical Analysis for Large Sample Sizes. PLoS Comput. Biol. 12(5): e1004842.

Kimura, M. 1953. “Stepping Stone” model of population. Ann. Rept. Nat. Inst. Genetics, Japan. 3: 62–63.

Kimura, M. 1968. Evolutionary rate at the molecular level. Nature. 217: 624–626.

Kimura, M. 1983. The Neutral Theory of Molecular Evolution. Cambridge Univ. Pres., Cambridge, UK.

Kimura, M. and G. Weiss. 1964. The stepping stone model of population structure and the decrease of genetic correlation with distance. Genetics. 49: 561–576.

King, J.L., and T.H. Jukes. 1969. Non-Darwinian evolution. Science. 164: 788–798.

Knowlton, N. and L.A. Weigt. 1998. New dates and new rates for divergence across the Isthmus of Panama. Proc. B. 265(1412): 2257–2263.

Kubatko, L.S., and J.H. Degnan. 2007. Inconsistency of Phylogenetic Estimates from Concatenated Data under Coalescence. Sys. Bio. 56(1): 17–24.

Leaché, A., and Bouckaert, R. 2018. Species Trees Estimation with SNAPP: A Tutorial and Example. Workshop on Population and Speciation Genomics, Český Krumlov.

Lepage, T., Bryant, D., Philippe, H., and N. Lartillot. 2007. A general comparison of relaxed molecular clock models. Mol. Biol. Evo. 24(12): 2669–2680.

Li, J., Huang, J-P., Sukumaran, J., and L.L. Knowles. 2018. Microevolutionary processes impact macroevolutionary patterns. BMC Evo. Bio. 18: 123.

Lynch, M. 1990. The rate of morphological evolution in mammals from the standpoint of the neutral expectation. Am. Nat. 136(6): 727–741.

Lynch, M. 2007. The Origins of Genome Architecture. Sinauer Associates, Inc. Sunderland, MA.

Magallón, S. 2010. Using Fossils to Break Long Branches in Molecular Dating: A Comparison of Relaxed Clocks Applied to the Origin of Angiosperms. Sys. Bio. 59(4): 384–399.

Malécot, G. 1968. The Mathematics of Heredity. Translated from the French edition (Paris, 1948). Ed. Yermanos, D.M. Freeman, San Francisco, 1969.

Maruyama, T. 1970a. Effective number of alleles in a subdivided population. Theo. Pop. Bio. 1: 273–306.

Maruyama, T. 1970b. The rate of decrease of heterozygosity in a population occupying a circular or linear habitat. Genetics. 67: 437–454.

Maruyama, T. 1971. Analysis of population structure: II. Two-dimensional stepping stone models of finite length and other geographically structured populations. Ann. Hum. Gen., Lon. 35: 179–196.

Meirmans, P.G. 2012. The trouble with isolation by distance. Mol. Eco. 21(12): 2839–2846.

Miller, M.A., Pfeiffer, W., and T. Schwartz. 2010. Creating the CIPRES Science Gateway for inference of large phylogenetic trees. Proceedings of the Gateway Computing Environments Workshop (GCE). New Orleans, LA.

Nei, M., and W.H. Li. 1979. Mathematical model for studying genetic variation in terms of restriction endonucleases. PNAS. 76(10): 5269-5273.

Peterson, M.A., and R.F. Denno. 1998. The influence of dispersal and diet breadth on patterns of genetic isolation by distance in phytophagous insects. Am. Nat. 152(3): 428–446.

Pond, S.K., and S.V. Muse. 2005. Site-to-site variation of synonymous substitution rates. Mol. Biol. Evo. 22(12): 2375–2385.

R Core Team (2019). R: A language and environment for statistical computing. R Foundation for Statistical Computing, Vienna, Austria. URL: https://www.R-project.org/.

Rieman, B.E., and F. W. Allendorf. 2011. Effective Population Size and Genetic Conservation Criteria for Bull Trout. North American Journal of Fisheries Management. 21(4): 756–764.

Rosenberg, N.A., and M.W. Feldman. 2002. The relationship between coalescent times and population divergence times. In: Modern Developments in Theoretical Population Genetics. Eds. Slatkin, M. and M. Veuille. Oxford Univ. Pres. New York, NY.

Slatkin, M. 1991. Inbreeding coefficients and coalescence times. Genet. Res., Camb. 58: 167–175.

Slatkin, M. 2004. Seeing ghosts: the effect of unsampled populations on migration rates estimated for sampled populations. Mol. Eco. 14(1): 67–73.

Stange, M., Sánchez-Villagra, M.R., Salzburger, W., and M. Matschiner. 2018. Bayesian divergence-time estimation with genome-wide single-nucleotide polymorphism data of sea catfish (Ariidae) supports Miocene closure of the Panamanian Isthmus. Sys. Bio. 67(4): 681–699.

Turner, T.F., Wares, J.P., and J.R. Gold. 2002. Genetic Effective Size Is Three Orders of Magnitude Smaller Than Adult Census Size in an Abundant, Estuarine-Dependent Marine Fish (*Sciaenops ocellatus*). Genetics. 162(3): 1329–1339.

Wakeley, J. 1998. Segregating sites in Wright's island model. Theoret. Pop. Biol. 53:166–175.

555 Wakeley, J. 1999. Non-equilibrium migration in human history. Genetics. 153:1863–1871.
556
557 Wakeley, J. 2000. The effects of subdivision on the genetic divergence of populations and
558 species. Evolution. 54(4): 1092–1101.
559
560 Weir, J.T., and D. Schluter. 2008. Calibrating the avian molecular clock. Mol. Eco. 17: 2321–
561 2328.
562
563 Wilkins, J.F., and J. Wakeley. 2002. The coalescent in a continuous, finite, linear population.
564 Genetics. 161: 873–888.
565
566 Wright, S. 1931. Evolution in Mendelian populations. Genetics. 16(2): 97–159.
567
568 Wright, S. 1943. Isolation by distance. Genetics. 28:114–138.
569
570 Yu, G., Smith, D.K., Zhu, H., Guan, Y., and T.T.Y. Lam. 2017. ggtree: an R package for
571 visualization and annotation of phylogenetic trees with their covariates and other associated data.
572 Meth. Eco. Evo. 8(1): 28–36.

573 **Supplementary Material**
574
575
576 **Table S1.** Pairwise Wilcoxon test results for comparisons of T_D / *ND* of 10, 5, 2, 1, 0.5, and 0.1.
577 Significant ($p < 0.05$) results are bolded.
578

Comparison	Ratio	Migration rate	p-value
Ends-Center	10	0.1	**<2E-16**
Island-Center	10	0.1	0.26
Island-Ends	10	0.1	**<2E-16**
Ends-Center	10	0.01	**<2E-16**
Island-Center	10	0.01	**0.019**
Island-Ends	10	0.01	**<2E-16**
Ends-Center	10	0.001	**<2E-16**
Island-Center	10	0.001	**0.00000012**
Island-Ends	10	0.001	**<2E-16**
Ends-Center	5	0.1	**<2E-16**
Island-Center	5	0.1	0.22
Island-Ends	5	0.1	**<2E-16**
Ends-Center	5	0.01	**<2E-16**
Island-Center	5	0.01	0.18

Island-Ends	5	0.01	**<2E-16**
Ends-Center	5	0.001	**<2E-16**
Island-Center	5	0.001	**1.2E-08**
Island-Ends	5	0.001	**<2E-16**
Ends-Center	2	0.1	**2.1E-11**
Island-Center	2	0.1	0.46
Island-Ends	2	0.1	**1.2E-10**
Ends-Center	2	0.01	**<2E-16**
Island-Center	2	0.01	**0.029**
Island-Ends	2	0.01	**<2E-16**
Ends-Center	2	0.001	**<2E-16**
Island-Center	2	0.001	**0.000041**
Island-Ends	2	0.001	**<2E-16**
Ends-Center	1	0.1	**0.0000038**
Island-Center	1	0.1	0.33893
Island-Ends	1	0.1	**0.00017**
Ends-Center	1	0.01	**<2E-16**
Island-Center	1	0.01	0.53

Island-Ends	1	0.01	**<2E-16**
Ends-Center	1	0.001	**<2E-16**
Island-Center	1	0.001	**0.0000023**
Island-Ends	1	0.001	**<2E-16**
Ends-Center	0.5	0.1	**0.027**
Island-Center	0.5	0.1	0.759
Island-Ends	0.5	0.1	**0.013**
Ends-Center	0.5	0.01	**<2E-16**
Island-Center	0.5	0.01	**0.032**
Island-Ends	0.5	0.01	**<2E-16**
Ends-Center	0.5	0.001	**<2E-16**
Island-Center	0.5	0.001	0.25
Island-Ends	0.5	0.001	**<2E-16**
Ends-Center	0.1	0.1	1
Island-Center	0.1	0.1	1
Island-Ends	0.1	0.1	1
Ends-Center	0.1	0.01	**0.0000068**
Island-Center	0.1	0.01	0.91

Island-Ends	0.1	0.01	**0.0000068**
Ends-Center	0.1	0.001	**<2E-16**
Island-Center	0.1	0.001	0.077
Island-Ends	0.1	0.001	**<2E-16**

Table S2. Wilcoxon pairwise test comparing ($T_{MRCA} - T_D$) / T_D of center and end demes for different rates of migration and ratios of T_D / *ND*. Bolded *p*-values indicate $p < 0.05$.

Ratio	Migration_rate	p-value
50	0.1	0.385
50	0.01	**0.000748**
50	0.001	**2.00E-16**
25	0.1	**0.00282**
25	0.01	**3.55E-09**
25	0.001	**2.00E-16**
10	0.1	**0.0118**
10	0.01	**1.24E-08**
10	0.001	**2.00E-16**
5	0.1	0.744
5	0.01	0.0528
5	0.001	**2.00E-16**
1	0.1	0.0672
1	0.01	**2.00E-16**
1	0.001	**2.00E-16**

Table S3. Table of estimated divergence-times in SNAPP.

T_D / ND	Deme sampled	Migration rate	True Age (T_D)	Expected Estimate (eT_D)	Actual Estimate (T_{MRCA})	T_{MRCA} - eT_D	(T_{MRCA} - eT_D) / eT_D
50	End	0.1	50000	52000	32929	-19071	-0.36675

50	End	0.01	50000	52000	36330	-15670	-0.301346154
50	End	0.001	50000	52000	40028	-11972	-0.230230769
50	Center	0.1	50000	52000	46270	-5730	-0.110192308
50	Center	0.01	50000	52000	54301	2301	0.04425
50	Center	0.001	50000	52000	49004	-2996	-0.057615385
25	End	0.1	25000	27000	25893	-1107	-0.041
25	End	0.01	25000	27000	26492	-508	-0.018814815
25	End	0.001	25000	27000	48430	21430	0.793703704
25	Center	0.1	25000	27000	22264	-4736	-0.175407407
25	Center	0.01	25000	27000	25488	-1512	-0.056
25	Center	0.001	25000	27000	26147	-853	-0.031592593
10	End	0.1	10000	12000	12439	439	0.036583333
10	End	0.01	10000	12000	14085	2085	0.17375
10	End	0.001	10000	12000	28629	16629	1.38575
10	Center	0.1	10000	12000	13234	1234	0.102833333
10	Center	0.01	10000	12000	13040	1040	0.086666667
10	Center	0.001	10000	12000	21782	9782	0.815166667
5	End	0.1	5000	7000	10618	3618	0.516857143

5	End	0.01	5000	7000	12730	5730	0.818571429
5	End	0.001	5000	7000	19936	12936	1.848
5	Center	0.1	5000	7000	11144	4144	0.592
5	Center	0.01	5000	7000	10595	3595	0.513571429
5	Center	0.001	5000	7000	11697	4697	0.671
1	End	0.1	1000	3000	1512.9	-1487.1	-0.4957
1	End	0.01	1000	3000	2700	-300	-0.1
1	End	0.001	1000	3000	23845	20845	6.948333333
1	Center	0.1	1000	3000	1513.2	-1486.8	-0.4956
1	Center	0.01	1000	3000	2649.1	-350.9	-0.116966667
1	Center	0.001	1000	3000	1647.2	-1352.8	-0.450933333

587

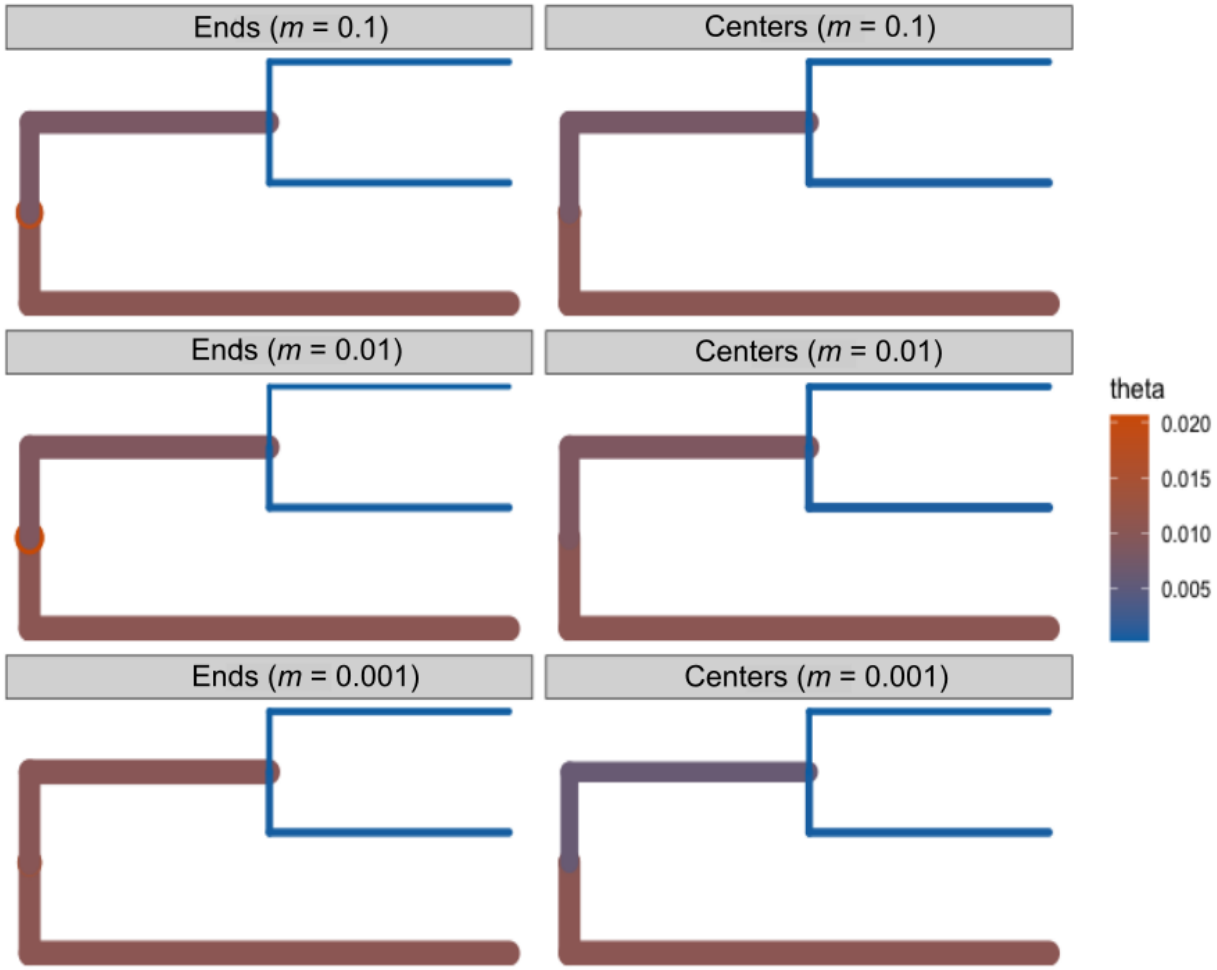

588

589

590 **Figure S1.** Estimates of θ in SNAPP for T_D / ND = 50. Branch widths are proportional to the
591 estimated θ.

592

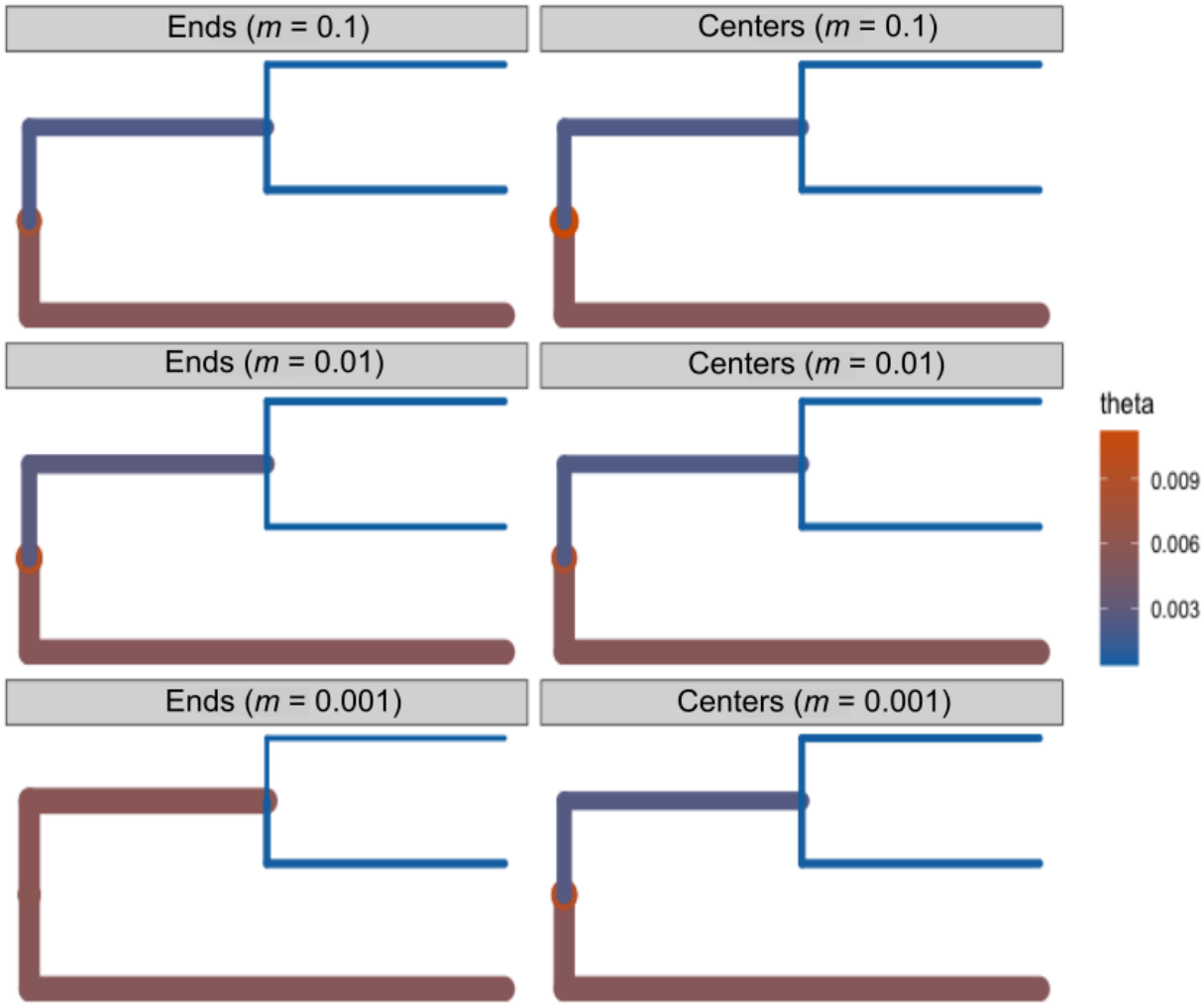

Figure S2. Estimates of θ in SNAPP for T_D / ND = 25. Branch widths are proportional to the estimated θ.

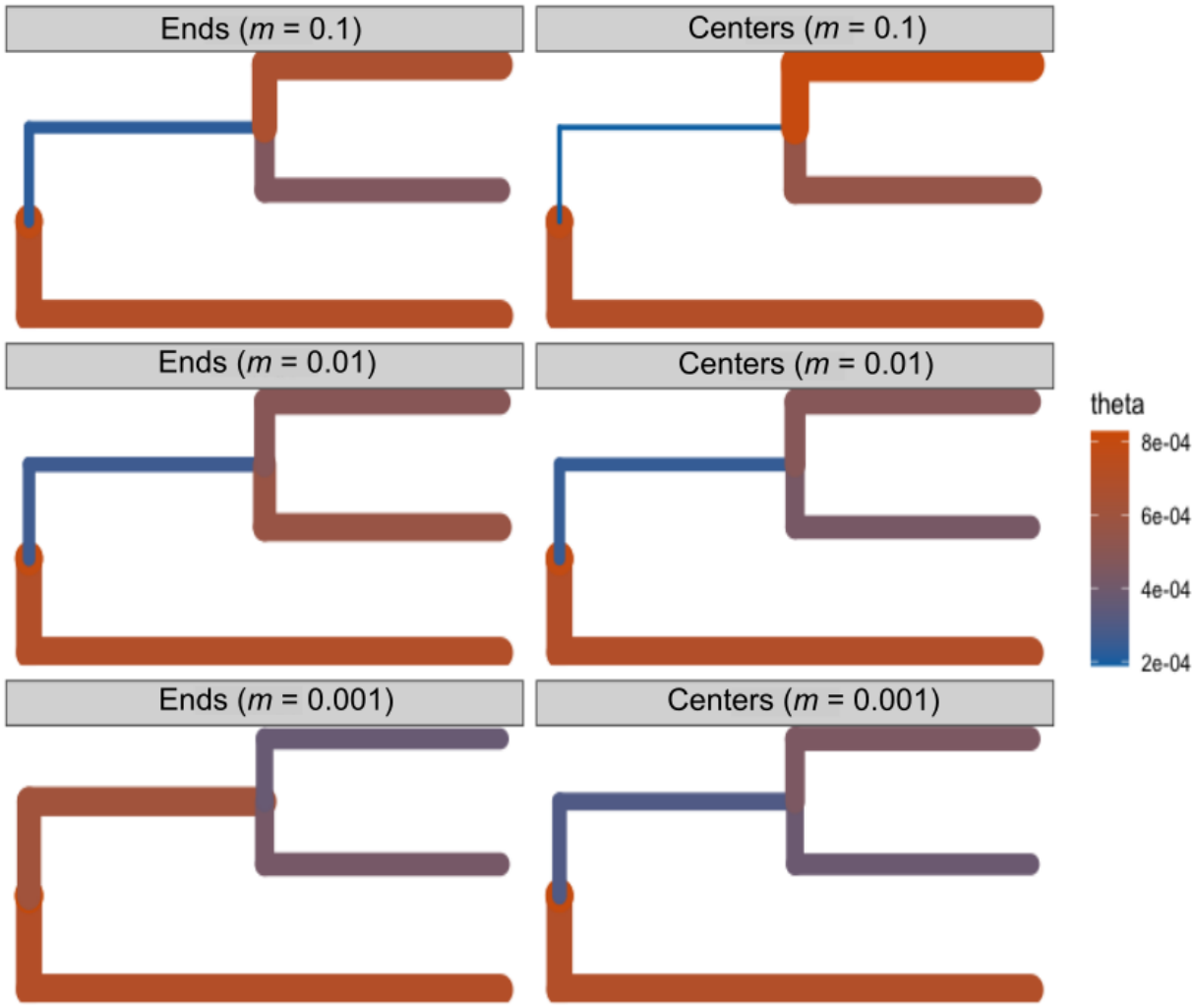

Figure S3. Estimates of θ in SNAPP for T_D / ND = 5. Branch widths are proportional to the estimated θ.

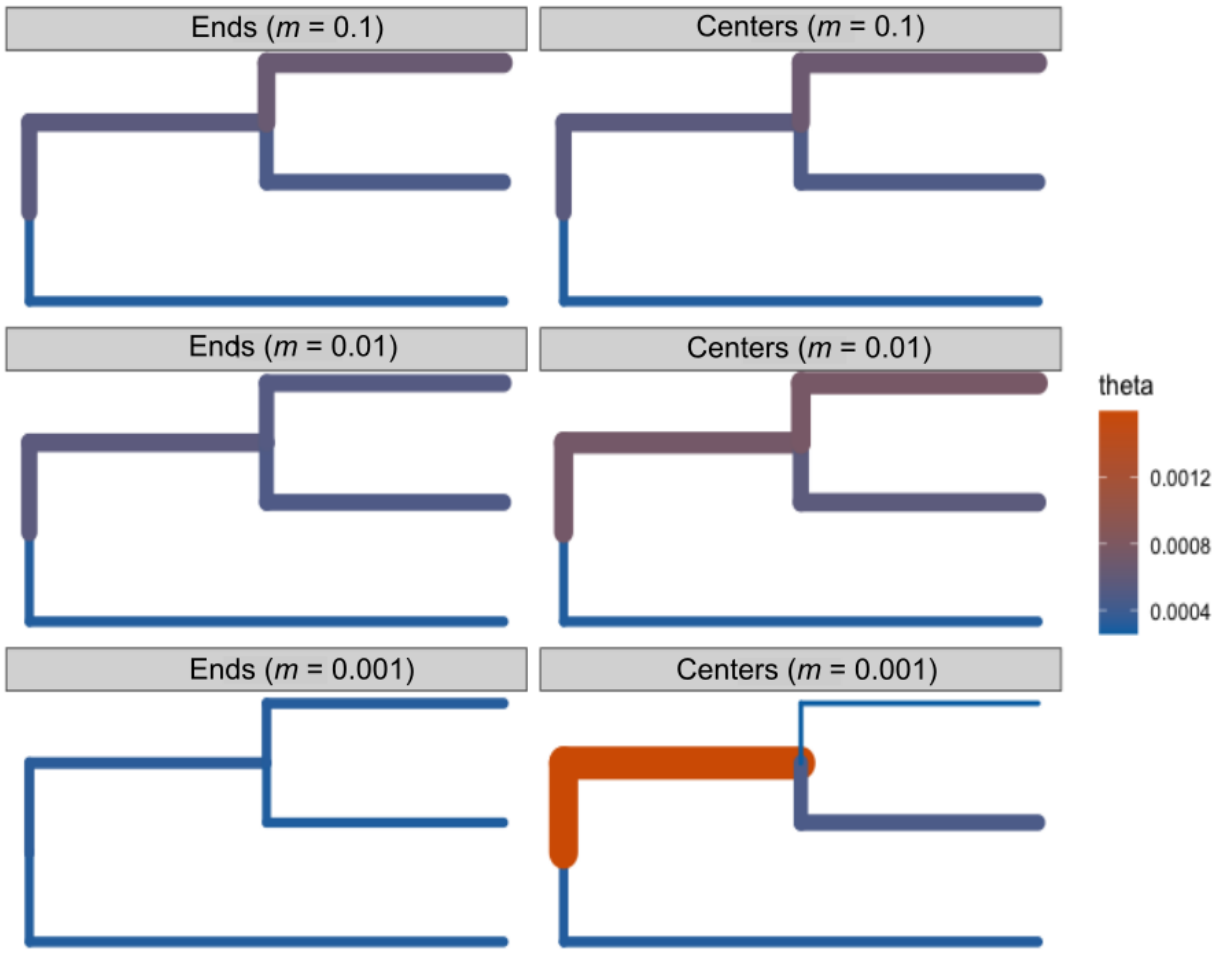

Figure S4. Estimates of θ in SNAPP for T_D / ND = 1. Branch widths are proportional to the estimated θ.

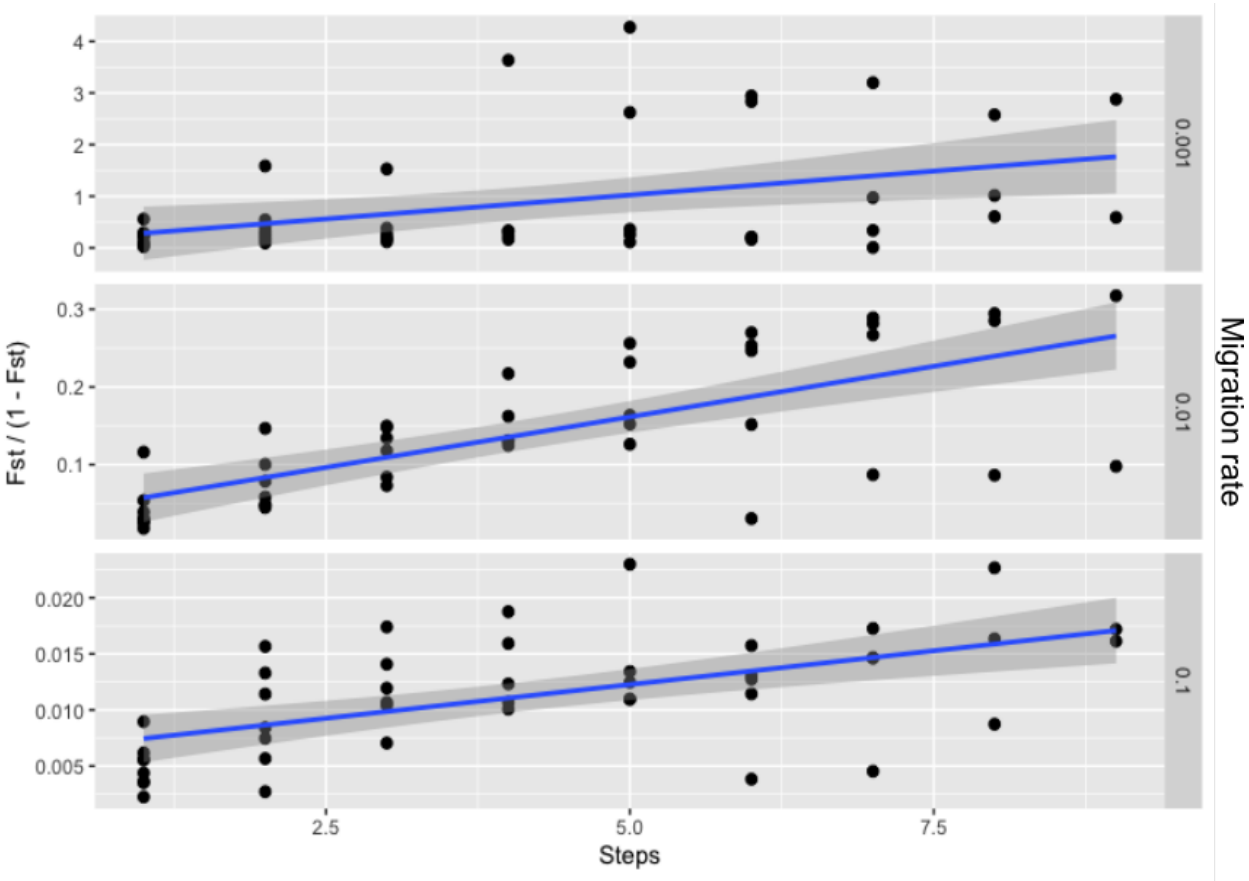

Figure S5. Isolation-by-distance plots for three migration rates in the ancestral population. Pairwise F_{ST} was calculated between each deme in the ancestral population prior to the split to verify that a pattern of IBD had occurred. "Steps" are the distance from deme *i* to deme *j*, where neighboring demes are 1 step apart. Note that the y-axis differs between panels. All slopes were significant ($p < 0.05$).